A Translating-Coil Magnetometer for the Magnetic Measurements of the HL-LHC High-Order Corrector Magnets at Room Temperature

M. Pentella ⓘ, E. Dalane ⓘ, E. De Matteis ⓘ, E. L. Gautheron ⓘ, S. Mariotto ⓘ, C. Petrone ⓘ, H. Prin ⓘ, M. Prioli ⓘ, S. Russenschuck ⓘ, M. Statera ⓘ, and E. Todesco ⓘ

Abstract—This article describes the design and development of a translating-coil magnetometer for the room-temperature magnetic measurements of the superferric, high-order corrector magnets for the high-luminosity upgrade of the Large Hadron Collider at CERN (HL-LHC). The measurement system consists of a set of induction coils, tangentially positioned on a measurement head. The translation of the measurement head yields an induced voltage proportional to the longitudinal field profiles of the magnets. In this way, it is possible to locate the longitudinal center and calculate the magnetic length. The measurements provide feedback to the assembly and fabrication processes. The metrological characterization of the induction-coil configurations is presented, and the measurement results are discussed in view of the target requirements of the HL-LHC project.

Index Terms—HL-LHC, high-order corrector package, translating-coil magnetometer, translating fluxmeter.

I. INTRODUCTION

THE high-order corrector package (CP) consists of nine high-order superferric magnets to be installed in the HL-LHC low-beta insertion region [1], [2], [3], [4]. The function of the CP is to correct for magnetic imperfections and misalignments of the focusing quadrupoles. Each corrector package will be installed symmetrically to the experiments and includes a skew quadrupole (a_2), a normal and a skew sextupole (b_3, a_3), a normal and a skew octupole (b_4, a_4), a normal and a skew decapole (b_5, a_5), and a normal and a skew dodecapole (b_6, a_6), disposed in the order shown in Fig. 1. The corrector package coldmass also includes an orbit corrector dipole, MCBXFA [5]. The nominal parameters of each magnet are summarized in Table I, at a reference radius of 50 mm.

After a series of measurements on prototypes at LASA and CERN [7], [8] and the roll-out of the series production with
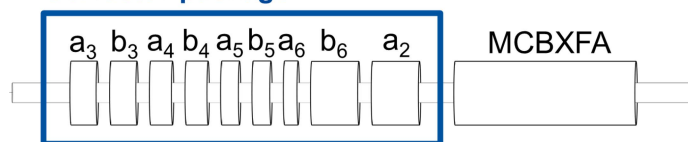
Corrector package

Fig. 1. Layout of the HL-LHC corrector package.

TABLE I
MAIN PARAMETERS OF THE HL-LHC CORRECTOR PACKAGE FROM [6]

Magnet	Integrated main field (Tm)	Magnetic length (mm)	Coil peak field (T)	Stored energy (kJ)	Operating current (A)
a_2	0.700	401	3.53	36	174
b_3, a_3	0.064	168	2.14	1.2	99
b_4, a_4	0.046	145	2.06	1.1	102
b_5, a_5	0.026	145	1.73	0.5	92
a_6	0.017	99	1.44	0.9	84
b_6	0.086	469	1.44	7.8	85

industrial partners [6], [9], the first batch of magnets was shipped to CERN for the assembly of the first coldmass. In this phase, knowledge of the magnetic axis, roll angle, magnetic length, and longitudinal center of each magnet is crucial for the correct positioning of each magnet in the assembly, and the installation of the coldmass in the machine. These parameters must be determined through room temperature measurements, which constitute a challenge from a metrological point of view, because the excitation current must be limited to about 1/1000 of the nominal value at 1.9 K. Consequently, the field levels are on the order of 1 mT. This article addresses the identification of the longitudinal centers and magnetic lengths. The measurement requirement in terms of 3-σ standard deviation is 10 mm [10] for the longitudinal center.

II. THE TRANSLATING-COIL MAGNETOMETER

A. Measurement Principle

The measurement principle is based on a flux-metric method, where flux variations are measured using an induction coil. If an induction coil is moved inside a magnetic field **B**, at a velocity

v, the induced voltage at the coil terminals is

$$u = \int_{\partial A} (\mathbf{v} \times \mathbf{B}) \cdot d\mathbf{r}, \tag{1}$$

where ∂A is the boundary enclosing the coil surface A and $d\mathbf{r}$ the line element.

This measurement principle has been exploited to obtain field maps of accelerator magnets. Examples of applications for solenoid magnets and spectrometer dipoles can be found in [11], [12]. The idea in both applications is to move the coil along the magnet's longitudinal axis from a zero-field region (outside the magnet fringe field) to a high-field region in the magnet center. Starting the scan from a zero-field region is crucial to capture the field profile accurately. If the scan were started in the high-field region, the induction coil would measure almost zero voltage because the field inside a magnet is usually homogeneous along the longitudinal axis.

B. Transducer Design

Modeling the magnet aperture as a cylindrical domain, the field in the CP magnets can be decomposed into a radial B_r and an angular component B_φ. The two field components can be described using the Fourier's series expansion around a circumference of radius r_0 [13]

$$B_r(r_0, \varphi) = \sum_{n=1}^{\infty} (B_n \sin(n\varphi) + A_n \cos(n\varphi)) \tag{2}$$

$$B_\varphi(r_0, \varphi) = \sum_{n=1}^{\infty} (B_n \cos(n\varphi) - A_n \sin(n\varphi)), \tag{3}$$

where the coefficient B_n and A_n are known as the *field harmonics* or *multipoles*.

In contrast with a rotating coil, where a coil rotates within the magnet bore and samples the field at various angular positions during rotation, the translating-coil magnetometer employs a set of equispaced fixed coils mounted on a cylindrical head. This configuration allows simultaneous sampling of the entire field distribution as the magnet is being scanned. Since the maximum harmonic order to be measured is six, the magnetometer comprises 12 induction coils spaced by an angular distance of $30°$. To further increase the sensitivity (field harmonics scale with r^{n-1} where n is the multipole order and r the measurement radius), the cylindrical head has the largest possible diameter compatible with the cold bore tube dimensions, which has a diameter of 136.5 mm. Each coil is realized through Printed Circuit Board (PCB) technology and has a calibrated area of 0.0594 m^2 [14], and consists of 132 turns printed on a 16-layer board, having a size of 40 mm × 20 mm. Finally, a Hall sensor is installed on one of the PCBs to pre-align the magnetometer to the maximum field. Fig. 2 shows a photograph of the measurement head.

Besides the measurement head, the rest of the assembly is identical to the one in [11]. The cylindrical head containing the coils is attached to a moving rod made of carbon fiber square tubes. A flange with a square hole is used to prevent the rod, and therefore the measurement head, from rotating during the translation.

Fig. 2. Photograph of the measurement head. In green, the PCB induction coils.

C. Measurement Procedure

The measurement procedure consists of powering one or more magnets of the CP assembly and manually displacing the magnetometer along the magnet's longitudinal axis. Each coil intercepts the flux variations arising from the movement, and the induced voltage is acquired by a Fast Digital Integrators (FDI) [15]. All the FDIs are simultaneously triggered. The FDIs acquire at a rate of 500 kHz and integrate between two consecutive triggers using the trapezoidal rule, obtaining the flux increments $\Delta\Phi$. The triggers for the FDIs, can be generated either by a draw-wire encoder or a laser tracker, thus linking the flux variations to the position of the measurement head.

The radial field component at the position z_k measured by the coil j, $B_{r,j}(z_k)$, can be obtained in two ways: i) by dividing the flux $\Phi_{r,j}(z_k)$ by the coil surface A_j or; ii) by deconvoluting the measured signal using the coil sensitivity function in the spatial frequency domain. The measured field profile is a moving average of the measurand profile, where the coil area is the averaging window.

Deconvolution is the inverse operation of the moving average, aiming to obtain the field profile, thus improving the accuracy of the measurement in correspondence with the regions where dB/dz is higher. In this article, the deconvolution was performed by iteratively reconstructing the field profile using b-splines. Both post-processing methods are compared in Section II-D.

The measurements were performed at a current level on the order of 100 mA, with main field levels of about 1 mT. At these low magnetizing currents, the remanent field from the iron magnetization has a non-negligible impact, up to 20% of the measured field. For this reason, each field scan has two repetitions, with the second performed after reversing the current polarity. The resulting field map is then obtained by a semi-difference of the two scans.

Once the field scan is completed, the magnet longitudinal center z_c is found by solving the following equation,

$$\int_{z_0}^{z_c} B_r dz = \int_{z_1}^{z_c} B_r dz, \tag{4}$$

where z_0 and z_1 are two symmetrical points on the magnet longitudinal axis at which the field can be assumed to be zero.
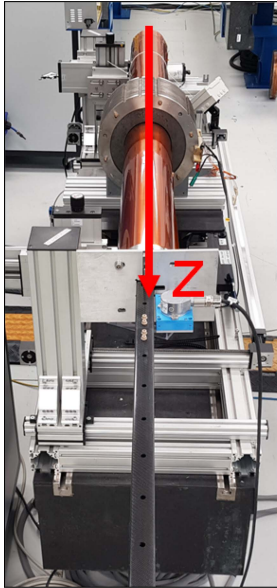
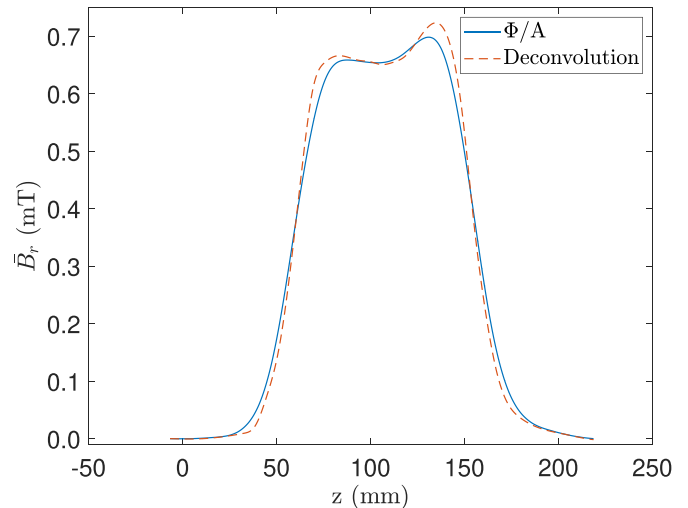Fig. 3. Measurement setup for the metrological characterization.

Fig. 4. Radial field profile for the decapole magnet as a function of the longitudinal position, averaged over the 12 induction coils. In blue (continuous line) and in red (dashed line), the two profiles calculated using the two post-processing algorithms.

The magnetic length l_m can be calculated as

$$l_m = \frac{\int_{z_0}^{z_1} B_r \mathrm{d}z}{B_r(z_c)}. \tag{5}$$

An additional post-processing step is to average the field profiles measured by the induction coils, in order to reduce the effect of mechanical instabilities on z_c and l_m. This averaging process operates under the assumption that when there is a transverse movement of the measurement head, the variation detected by one coil is mirrored by the coil positioned $180°$ apart, albeit with the opposite sign. In simpler terms, if a transverse movement causes a decrease in signal voltage for one coil, the coil positioned $180°$ away will measure an increase in signal voltage of equal magnitude. For the sake of clarity, an average of all the signals would result in zero because the field levels follow a sinusoidal distribution as a function of the angular position of the coils. Therefore, the sign of half of the signals is inverted before the average.

D. Metrological Characterization

The metrological characterization was performed on a dedicated test bench in a temperature-controlled environment by measuring a decapole prototype magnet. Fig. 3 shows a picture of the test bench setup.

Fig. 4 shows the flux density profiles averaged over the induction coils, $\bar{B}_r$ for both post-processing methods, measured at an excitation current of 105 mA. According to the parameters reported in [16] for the prototypes, the magnet prototype is geometrically shorter than the series one (233 mm against 246 mm), and it has a lower magnetic length (97 mm against 145 mm). A Leica AT960 laser tracker [17] was used to trigger the integrators and measure the position of the measurement head.

From the measured profile, it can be observed that the field presents peaks near the two magnet ends. The two peaks are due

TABLE II
MAGNETIC CENTER AND LENGTH FOR THE DECAPOLE MAGNET

	Value (Φ/A)	3-σ std. (Φ/A)	Value (Deconvolution)	3-σ std. (Deconvolution)
z_c (mm)	109.4	0.9	109.4	0.9
l_m (mm)	103.9	0.6	103.5	1.2

to the fact that at such a current level, the magnet pole can be considered to have a high uniform permeability without saturation effects, and the sharp edges of the poles determine the local increase of the field. The field profile evaluated by deconvoluting the signals from the induction coils presents higher peak values by a few $10\,\mu$T and a higher gradient from zero to the central field region. The effect was expected since the averaged field profile (Φ/A) is a moving average of the deconvoluted one. However, the deconvoluted profile exhibits some oscillations because of the coil's blind eye to high spatial frequencies [12].

Table II reports the magnetic center and magnetic length values evaluated using both post-processing methods.

The post-processing algorithm does not significantly impact the estimation of the magnetic center z_c. This outcome was expected because the magnet center displays a flat behavior, and the deconvoluted profile does not differ significantly from the averaged one in that region. On the other hand, the magnetic lengths present a difference of 0.4 mm, which is not significant given the values of the standard deviations. This difference can be explained by a non-perfect flat profile at the magnet center, where the central field values slightly differ between both computed profiles.

Compared with the geometric center at 116.5 mm, the magnetic center differs by 7.1 mm, which is within the requirement for HL-LHC. Similarly, the magnetic length is longer by 6 mm with respect to the expected value, 97 mm, which is again within the requirements.
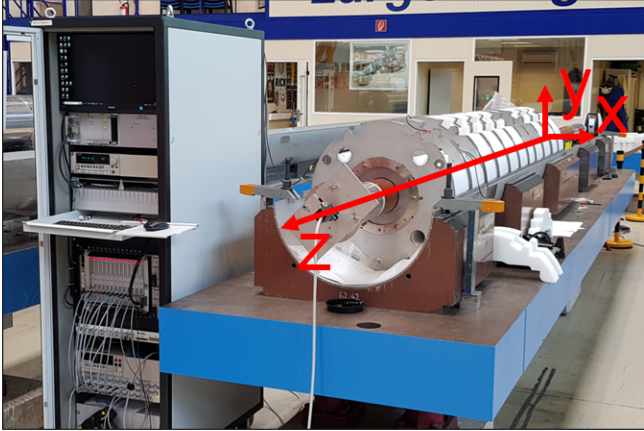
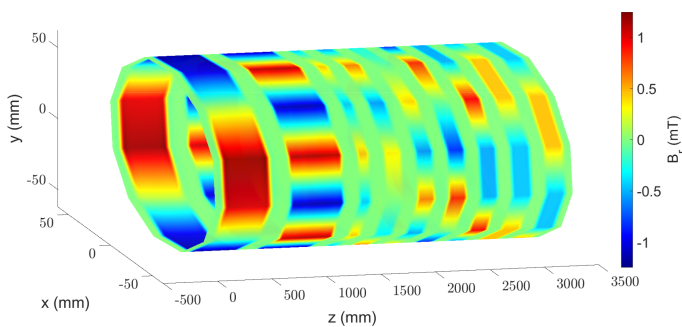Fig. 5. Measurement setup for the mapping of the CP assembly.

Fig. 6. Measured radial field component as a function of the longitudinal position. From $z = 0$, the magnet order follows the order listed in Table III.
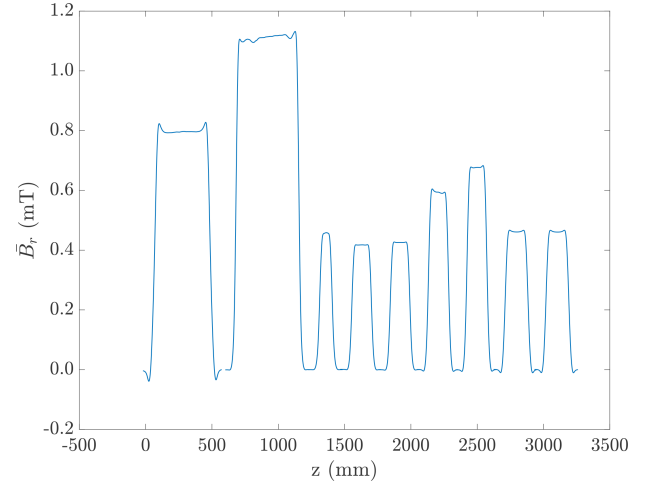

Fig. 7. Radial field component averaged over the 12 induction coils as a function of the longitudinal position. From $z = 0$, the magnet order follows the order listed in Table III.

TABLE III
MEASURED VALUES OF THE MAGNETIC CENTERS AND MAGNETIC LENGTHS
FOR THE CP ASSEMBLY

Magnet	Magnetic center (mm)	Magnetic length (mm)	Geometric center (mm)	Magnetic length (nom.) (mm)
a_2	285.9±1.2	422.4±1.0	284.3	401
b_6	928.6±3.0	473.0±6.9	925.2	469
a_6	1368.4±4.5	96.9±3.7	1363.9	99
b_5	1637.7±1.0	150.5±1.0	1633.7	145
a_5	1927.1±1.5	150.8±1.0	1923.4	145
b_4	2216.2±1.4	153.8±1.8	2213.1	145
a_4	2506.8±1.7	152.9±0.3	2502.9	145
b_3	2805.7±1.3	172.8±0.4	2801.6	168
a_3	3113.2±1.6	172.8±0.5	3109.2	168

III. MAGNETIC MEASUREMENT OF THE CP ASSEMBLY

Fig. 5 shows the measurement setup used for the mapping of the CP assembly, which is identical to the one presented in Section II-D. Since the CP assembly was measured with all the magnets powered at once, the excitation current used for the measurement was 60 mA due to power-supply limitations in feeding current to the series of magnets.

Figs. 6 and 7 show the measured field map, with all main field components visible. The values of the magnetic centers and lengths are given in Table III, together with their 3-σ standard deviations. Deconvolution was not applied, given its negligible impact on the estimation of magnetic center and length.

The field maps shown in Fig. 6 highlight the capability of the measurement system to capture all the harmonic orders in the CP assembly. The resulting magnetic centers and lengths presented in Table III are within the measurement requirements. The only exception is the deviation of the quadrupole magnetic length from the nominal value, which is about 21 mm.

IV. CONCLUSION

In this article, the design, characterization, and operation of a translating-coil magnetometer are presented in order to determine the magnetic center and length of the high-order corrector package magnets during the assembly. The measured centers match the geometric ones and are within the uncertainty requirements. The magnetic lengths display a larger deviation with respect to the nominal values, although not significant. The only exception is the quadrupole magnet, displaying a deviation of 21 mm from the nominal magnetic length. This deviation in the magnetic length may arise from the fact that the simulations were performed at nominal current, where the iron yoke is heavily saturated, thus impacting the magnetic length value.

In conclusion, the system is capable of meeting the measurement requirements in terms of magnetic center and length. In terms of field maps, the coil length determines a limited longitudinal resolution, resulting in field maps being the moving average across the measurand. To improve this aspect of the measurement system, a new PCB array of induction coils with a layout similar to the one presented in [11] is being designed and produced.

REFERENCES

[1] P. Abramian et al., "Development of superconducting corrector magnets with hard radiation resistance for LHC upgrade," *IEEE Trans. Appl. Supercond.*, vol. 23, no. 3, Jun. 2013, Art. no. 4101204.

[2] E. Todesco et al., "A first baseline for the magnets in the high luminosity LHC insertion regions," *IEEE Trans. Appl. Supercond.*, vol. 24, no. 3, Jun. 2014, Art. no. 4003305.

[3] G. Volpini et al., "NbTi superferric corrector magnets for the LHC luminosity upgrade," *IEEE Trans. Appl. Supercond.*, vol. 25, no. 3, Jun. 2015, Art. no. 4002605.

[4] E. Todesco et al., "The high luminosity LHC interaction region magnets towards series production," *Supercond. Sci. Technol.*, vol. 34, no. 5, 2021, Art. no. 053001.

[5] C. M. Jardim et al., "First short orbit nested corrector magnet for HL-LHC produced in the industry," *IEEE Trans. Appl. Supercond.*, vol. 33, no. 5, Aug. 2023, Art. no. 9000505.

[6] M. Statera et al., "Experience on series production of the HL-LHC superferric high order corrector magnets," *IEEE Trans. Appl. Supercond.*, vol. 33, no. 5, Aug. 2023, Art. no. 4004007.

[7] L. Fiscarelli et al., "Magnetic measurements on the prototype magnets of the high-order correctors for HL-LHC," *IEEE Trans. Appl. Supercond.*, vol. 29, no. 5, Aug. 2019, Art. no. 4003505.

[8] E. De Matteis et al., "Magnetic measurements results and analysis of the first batches of superferric magnets for the HL-LHC high order field correction," *IEEE Trans. Appl. Supercond.*, vol. 32, no. 6, Sep. 2022, Art. no. 4004905.

[9] E. Todesco et al., "Status and challenges of the interaction region magnets for HL-LHC," *IEEE Trans. Appl. Supercond.*, vol. 33, no. 5, Aug. 2023, Art. no. 4001608.

[10] M. Giovannozzi, S. Fartoukh, and R. De Maria, "Specification of a system of correctors for the triplets and seperation dipoles of the LHC upgrade," CERN, Geneva, Switzerland, Tech. Rep. CERN-ACC-2013-0168, 2013.

[11] C. Petrone, S. Sorti, E. Dalane, B. Mehl, and S. Russenschuck, "Induction-coil measurement system for normal-and superconducting solenoids," *IEEE Trans. Appl. Supercond.*, vol. 32, no. 6, Sep. 2022, Art. no. 9000605.

[12] M. Liebsch, S. Russenschuck, and J. Kaeske, "An induction-coil magnetometer for mid-plane measurements in spectrometer magnets," *Sensors Actuators A: Phys.*, vol. 355, 2023, Art. no. 114334.

[13] S. Russenschuck, *Field Computation for Accelerator Magnets: Analytical and Numerical Methods for Electromagnetic Design and Optimization*. Hoboken, NJ, USA: Wiley, 2011.

[14] P. Arpaia et al., "Drift-free integration in inductive magnetic field measurements achieved by Kalman filtering," *Sensors*, vol. 22, no. 1, 2021, Art. no. 182.

[15] P. Arpaia, L. Bottura, L. Fiscarelli, and L. Walckiers, "Performance of a fast digital integrator in on-field magnetic measurements for particle accelerators," *Rev. Sci. Instrum.*, vol. 83, no. 2, 2012, Art. no. 024702.

[16] M. Sorbi et al., "Status of the activity for the construction of the HL-LHC superconducting high order corrector magnets at LASA-Milan," *IEEE Trans. Appl. Supercond.*, vol. 28, no. 3, Apr. 2018, Art. no. 4100205.

[17] Hexagon, "Leica absolute tracker AT930," 2024. [Online]. Available: https://www.hexagonmi.com/products/laser-tracker-systems/leica-absolute-tracker-at930